Available online at www.sciencedirect.com
ScienceDirect
Nuclear Physics A 861 (2011) 47–66
NUCLEAR PHYSICS A
www.elsevier.com/locate/nuclphysa

Reaction mechanisms and staggering in S + Ni collisions

M. D'Agostino [a,*], M. Bruno [a], F. Gulminelli [b], L. Morelli [a], G. Baiocco [a,b], L. Bardelli [c,d], S. Barlini [c], F. Cannata [a], G. Casini [c], E. Geraci [e,d], F. Gramegna [f], V.L. Kravchuk [f], T. Marchi [f,g], A. Moroni [h], A. Ordine [i], Ad.R. Raduta [j]

[a] *Dipartimento di Fisica dell'Università and INFN, Bologna, Italy*
[b] *LPC (IN2P3-CNRS/Ensicaen et Université), F-14076 Caen cédex, France*
[c] *INFN, Firenze, Italy*
[d] *INFN, Catania, Italy*
[e] *Dipartimento di Fisica dell'Università, Catania, Italy*
[f] *INFN, Laboratori Nazionali di Legnaro, Italy*
[g] *Dipartimento di Fisica dell'Università, Padova, Italy*
[h] *INFN, Milano, Italy*
[i] *INFN, Napoli, Italy*
[j] *NIPNE, Bucharest-Magurele, POB-MG6, Romania*

Received 18 March 2011; received in revised form 2 May 2011; accepted 2 June 2011

Available online 7 June 2011

Abstract

The reactions $^{32}S + ^{58}Ni$ and $^{32}S + ^{64}Ni$ are studied at 14.5 A MeV. After a selection of the collision mechanism, we show that important even–odd effects are present in the isotopic fragment distributions when the excitation energy is small. Close to the multifragmentation threshold this staggering appears hidden by the rapid variation of the production yields with the fragment size. Once this effect is accounted for, the staggering appears to be a universal feature of fragment production, slightly enhanced when the emission source is neutron poor. A closer look at the behavior of the production yields as a function of the neutron excess $N - Z$, reveals that odd–even effects cannot be explained by pairing effects in the nuclear masses alone, but depend in a more complex way on the de-excitation chain.
© 2011 Elsevier B.V. All rights reserved.

* Corresponding author.
E-mail address: dagostino@bo.infn.it (M. D'Agostino).

0375-9474/$ – see front matter © 2011 Elsevier B.V. All rights reserved.
doi:10.1016/j.nuclphysa.2011.06.017

Keywords: NUCLEAR REACTIONS ^{58,64}Ni(^{32}S, X), $E = 463$ MeV; measured fragment yield and charge distribution; deduced reaction mechanism features, odd–even effects. Comparison with GEMINI evaporation model. GARFIELD detector array and ring counter

1. Introduction

Odd–even effects in fragment production have been experimentally investigated since a long time [1–5] but never quantitatively understood. This was observed in different reactions with different target–projectile combinations and in a large range of beam energies. It was found that the distributions of light fragmentation residues after violent heavy-ion collisions reveal an even–odd staggering of similar magnitude as in the case of low-energy reactions.

The odd–even anomaly was reported in the literature to be more pronounced in reactions involving Ni projectile and targets, in particular in n-poor systems, while in experiments involving Ca projectile and targets it was not observed up to the advent of experimental devices with very good accuracy of Z-identification [5–7].

In some experiments [1,3,4] the magnitude of the odd–even effect is found to be related to the isospin of the projectile and/or the target. The effect in final observables was seen to be very large in reactions where at least one of the reaction partner has $N - Z = 0$ (as ^{32}S). For $N - Z = 2$ systems, like ^{58}Ni, the staggering was found [1,3] to be small, and even smaller effects have been observed for systems with $N - Z \geqslant 4$.

We recall another interesting observation [3]: final odd-mass fragments show a strong reversed even–odd effect with enhanced production of odd-Z nuclei for $N - Z = 5$.

An even–odd staggering is also observed in many isotopic variables as the $\langle N \rangle / Z$ and the width of the isotopic distribution [4], almost independently of the target.

From a theoretical point of view, odd–even effects in fragmentation reactions are clearly linked to the pairing residual interaction and its dependence on temperature, which are very important quantities both in nuclear physics [8] and in nuclear astrophysics [9,10]. Understanding their origin is also important for studies on the symmetry energy [11–13], which can be linked to the isotopic distributions [14] if the latter are not too much perturbed by secondary decay [15,16].

In theoretical dynamical or statistical models no staggering is associated to the finite temperature yields, but odd–even effects may appear on the asymptotic yields after evaporation [12,13]. This observation suggests that odd–even effects are low temperature effects associated to the evaporation phase. Two physical ingredients which can be associated to odd–even effects exist in evaporation models, namely level densities and binding energies. Then the question arises whether the observed staggering in the production yields is just a trivial consequence of the pairing effect in nuclear masses.

This problem was recently raised in Ref. [3], where odd–even effects in the reaction $p + \mathrm{Fe}$ at 1 A GeV at the FRS were studied. The idea proposed in that paper is that indeed nuclear masses determine the observed staggering through the last step of the evaporation chain: the hypothesis made is that independently of the initial thermodynamical condition of the excited pre-fragments, the very last evaporation step concerns either a neutron or a proton depending on the relative separation energies of the two particles; the staggering in the yields would then reflect the staggering in the neutron–proton separation energies due to the pairing and Wigner term in the mass formula.

This idea predicts correctly the trend of the observed staggering in the experiment at the FRS. However it does not reproduce the amplitude of the staggering quantitatively: the experimental

oscillations are less important than the ones predicted in this simple scenario. This suggests that the previous evaporation steps may also play a role. This last suggestion agrees with the theoretical fact that ABLA calculations [17] show that a staggering is already present in the isotopic yields at the last but one evaporation step [18].

In this paper we report on an experimental study of staggering in S + Ni collisions at 14.5 A MeV. To explore in more detail the possible relationship of odd–even effects to the isospin of the emitting sources, we have measured the yields of isotopes for reaction pairs differing only in the values of the isospin. The choice of incident energies of about 15 A MeV allows to study excited sources at the threshold of multifragmentation (excitation energies ~ 3 A MeV). We expect that measurements of this kind, at the turning point of the caloric curve [19], should give important information on the thermal properties as a function of isospin in the vicinity of the liquid–gas phase transition. The selection of central fusion events, and peripheral quasi-projectile events, allows to further study the possible dependence of odd–even effects on the reaction mechanism and the excitation energy.

The main result of this paper is that the staggering does not only reflect the pairing effect on nucleon separation energies, but is also related to the spectroscopic structure of the high-lying particle unstable excited levels. Moreover, the importance of odd–even effects appears correlated to the mechanism of fragment emission. In particular, the opening of the multifragmentation channel has the effect of smearing such effects.

2. Experiment and data selection

The measurements were performed in the third experimental Hall at the Legnaro National Laboratory. A pulsed beam (around 1 ns FWHM) of ^{32}S provided by the TANDEM-ALPI acceleration system was used to bombard self-supporting ^{58}Ni and ^{64}Ni targets, 150 μg/cm^2 thick. The bombarding energy was 463 MeV. The grazing angle for these reactions was 8.6°.

The detecting device is composed by the GARFIELD detector [20] covering almost completely the angular range of polar angle from 30° to 85° and an annular three-stage detector (Ring Counter) [21] covering laboratory forward angles from 5.3° to 17.5°.

A complete description of the two devices is given in Refs. [20,21]. We recall here only the main characteristics of the apparatus.

GARFIELD is made by a drift chamber, filled with CF_4 gas at low pressure (about 50 mbar), azimuthally divided into 24 sectors, each one consisting of $8\Delta E - E$ telescopes, for a total of 192 telescopes.

The operation of the GARFIELD apparatus is largely based on the $\Delta E - E$ technique, in which the ΔE signal is given by the drift chamber, where gaseous micro-strip detectors collect and amplify the primary electrons produced along the ionization track of the detected particle. The CsI(Tl) scintillation detectors, lodged in the same gas volume, are used to get information on the residual energy.

The advantages of using micro-strip gas chambers are in the large dynamical range and high signal-to-noise ratio (Z identification from low energy protons up to highly ionizing heavy ions).

The Ring Counter [21] is designed to be centered at 0° with respect to the beam direction. It is an array of three-stage telescopes realized in a truncated cone shape. The first stage is an ionization chamber (IC), the second a 300 μm strip silicon detector (Si) and the last stage a CsI(Tl) scintillator.

The RCo has eight separate silicon detectors, pie shaped, each one segmented into eight independent annular strips on the front surface (junction side). The angular resolution of each of the 64 strips is $\pm 0.9°$, the geometrical coverage is about 90%.

The typical energy resolutions of the device are less than 0.5% FWHM for the silicon strips, 3–4% FWHM for the CsI crystals and of less than 10% FWHM for the gas detectors.

The whole detecting device operated in vacuum ($P = 10^{-6}$ Torr) with minimal outgassing.

The detecting device can identify from light charged particles to heavy fragments with an energy threshold of the order of few hundreds of keV/A.

To sort the measured events as a function of the centrality, we adopted the method of the "shape analysis" [22], common to other intermediate and high energy experiments performed with $\simeq 4\pi$ detectors [23,24].

To investigate the fragment emission patterns one has to construct the momentum tensor [22]:

$$T_{ij} = \sum \frac{p_i^{(n)} \cdot p_j^{(n)}}{p^{(n)}} \quad (i, j = 1, 2, 3) \tag{1}$$

where $p_i^{(n)}$, $p_j^{(n)}$ are the ith and jth Cartesian projections of the momentum $\vec{p}^{(n)}$ of the nth fragment in the center of mass frame. The sum runs over the number of charged products with ($Z \geqslant 2$) [25] detected in each event. The diagonalization of this tensor gives three eigenvalues λ_i and three eigenvectors $\vec{e}_i$. The event shape is an oriented ellipsoid with the principal axes parallel to the eigenvectors.

The flow angle θ_{flow} is defined as the angle between the eigenvector $\vec{e}_1$ for the largest eigenvalue λ_1 and the beam axis $\hat{u}_3$:

$$\cos(\theta_{flow}) = |\vec{e}_1 \cdot \hat{u}_3| \tag{2}$$

In order to perform the shape analysis it is necessary to select events where a considerable amount of the incoming momentum has been detected. Then the inspection of the correlation between the total detected charge and the flow angle will allow to separate central and peripheral events. The flow angle is indeed a variable sensitive to the dynamics of the fragmentation process. Specifically, the emission of fragments from only one source should be on the average isotropic in momentum space and the flow angle should have a flat distribution. Conversely in peripheral reactions the forward–backward emission of fragments from the quasi-projectile (QP) and quasi-target (QT) should lead to an event shape elongated along the beam axis and a flow angle peaked in the forward direction.

Calculations performed for our reactions with the dynamical event generator Hipse [26] confirm that the sorting of events in intervals of θ_{flow} corresponds to a classification in terms of impact parameter, due to the monotonic relationship between these two quantities. This correspondence is almost the same for model events filtered through a software replica of the apparatus, provided that well detected events, as defined below, are selected.

The first selection of measured events is presented in Fig. 1, where we show on the left panels the total detected charge as a function of the total longitudinal momentum, normalized to the projectile momentum, for the $^{32}S + ^{58}Ni$ (upper panel) and $^{32}S + ^{64}Ni$ reactions (lower panel). Asking that at least 50% of the total incoming parallel momentum is collected (dashed lines) allows to keep events with two distinct values of the total detected charge (right panels): the higher bump corresponds to an average detected charge about 80% of the total charge, the lower one corresponds to the detection of the QP, being the QT and its products undetected because of the energy thresholds.

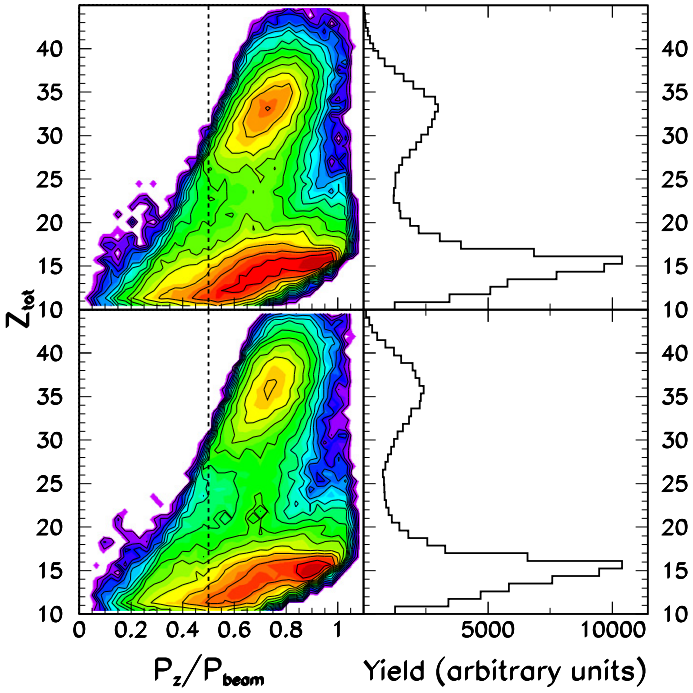

Fig. 1. (Color online.) Left panels: contour plot of the total detected charge as a function of the total longitudinal momentum normalized to the projectile momentum for $^{32}S + ^{58}Ni$ (upper part) and $^{32}S + ^{64}Ni$ (lower part). Darker shades represent increasing yield (in a logarithmic scale). Right panels: projection on the Z_{tot} axis of events satisfying the requirement: $P_z/P_{beam} \geqslant 0.5$ (dashed line in the left panels).

On the left of the dashed line corresponding to our first selection, events lie which are poorly detected from the point of view of the total detected charge and total detected linear momentum. In the following we analyze events under the condition $P_z \geqslant 0.5 \cdot P_{beam}$. To establish further selections on the total measured charge and define, for our data, "well detected events", we examine in Fig. 2 (panel a) the behavior of the total detected charge as a function of the "flow angle" for the n-poor system. The behavior is the same for the n-rich one. As in the case of other light systems [25], the flow angle was calculated for events where at least one fragment ($Z \geqslant 3$) and one α-particle have been detected.

We observe (panel (a) of Fig. 2) that peripheral events, characterized by a total detected charge close to the projectile charge, keep a strong memory of the entrance channel and are therefore restricted to low value of the flow angle.

Larger values of the total charge are distributed over the whole range of θ_{flow} with nearly constant statistics, which implies a nearly flat distribution of $\cos(\theta_{flow})$, as expected for spherical events.

A first glimpse on the topology of the events can be inferred from panel (b) of Fig. 2, which displays the correlation between the flow angle and the charge of the heaviest fragment measured in each event. For high values of the total charge, thus excluding QP contributions, and $\cos(\theta_{flow}) \geqslant 0.5$ the largest fragment has a charge close to the total charge, as expected from an evaporation residue. For decreasing $\cos(\theta_{flow})$, we observe a decrease of the largest fragment,

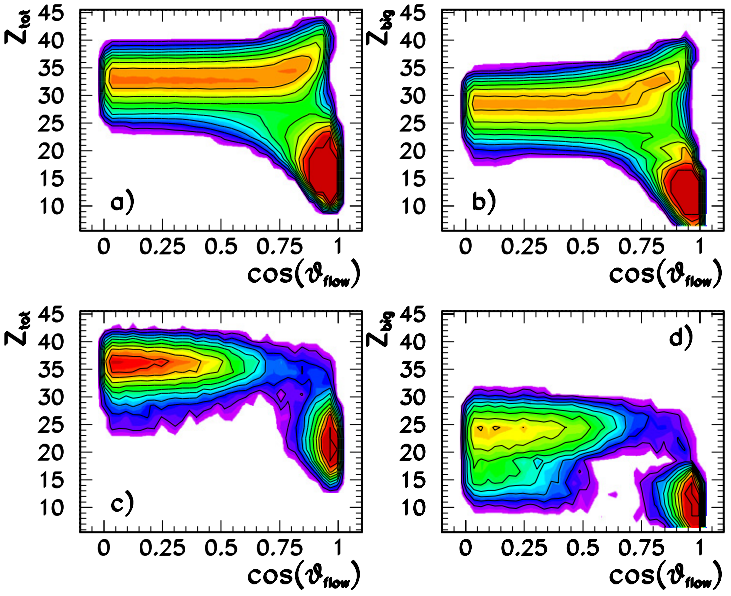

Fig. 2. (Color online.) Contour plot of the total detected charge (left panels) and charge of the largest fragment (right panels) as a function of the cosinus of the flow angle for $^{32}S + ^{58}Ni$ under the condition: $P_z/P_{beam} \geqslant 0.5$. Darker shades represent increasing yield (in a logarithmic scale). Upper part (panels (a), (b)): all events. Lower part (panels (c), (d)): events with at least three detected fragments with $Z \geqslant 3$. For a better visualization of events with high value of the total charge, a maximum histogram content has been set, limiting only the yield of peripheral events.

suggesting higher excitation. This corresponds in the measured partitions to an increase of the multiplicity of emitted charged products.

The lower part of Fig. 2 shows that the evaporation phenomenon coexists with many fragment production: for the most dissipative collisions a small fraction (about 5%) of well measured central events corresponds to 3 or more fragment ($Z \geqslant 3$) events. These events are characterized by increasing values of the "flow angle" [23] for increasing fragment multiplicity.

Some three-fragment events are also associated to peripheral collisions. The fact that the distribution of the largest fragment is not sensitively affected by the fragment multiplicity indicates that fragments emitted by the target can be detected together with the QP products [27].

After the inspection of Fig. 2 we can set the final event selections to study central and peripheral collisions for our data set. For the analyses presented in the following, besides the condition on the total longitudinal momentum, central events are also defined by a lower threshold of the total detected charge: $Z_{tot} \geqslant 70\% \cdot Z_{S+Ni}$.

Peripheral events are analyzed by setting an upper threshold of the total detected charge $Z_{tot} \leqslant 25$. To avoid contamination of non-peripheral events with low value of Z_{tot}, we also restrict the flow angle range: $\cos(\theta_{flow}) \geqslant 0.77$. Three-fragment events associated to selected peripheral collisions, correspond to a deposited energy, evaluated via calorimetry, of about 1 A MeV.

In Fig. 3 we display the flow angle distribution of central events corresponding to different fragment multiplicities for the n-poor system. The behavior is the same for the n-rich one. The distribution is almost isotropic, as expected for events corresponding to the decay of only one source, but kinematics as well as detection effects favor a backward emission for high multiplicity events. The measured percentage of many-fragment events (5%), that can be associated to

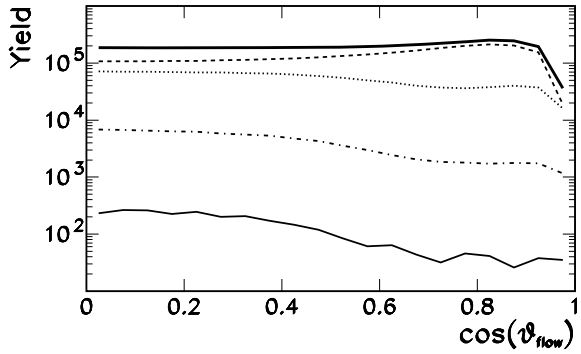

Fig. 3. Distribution of the cosinus of the flow angle for $^{32}S + ^{58}Ni$ well detected central events for different values of the fragment ($Z \geqslant 3$) multiplicity. Thick solid line represents the global distribution. Dashed, dotted, dot-dashed and solid thin lines correspond to fragment multiplicities 1, 2, 3, and larger than 3, respectively.

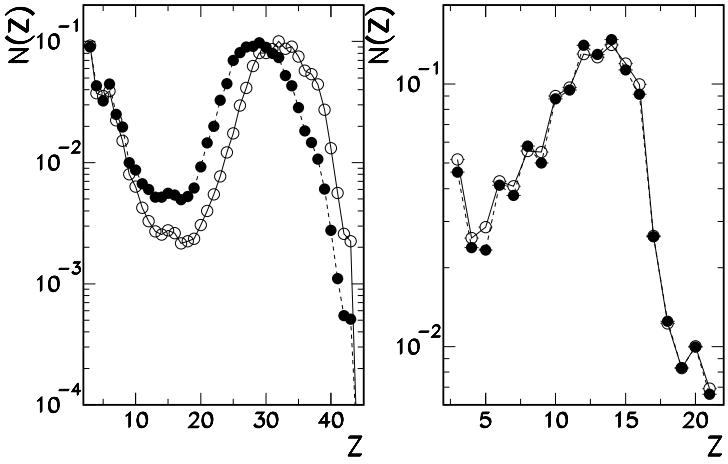

Fig. 4. Elemental fragment ($Z \geqslant 3$) distribution for $^{32}S + ^{58}Ni$ (full symbols, dashed line) and $^{32}S + ^{64}Ni$ (open symbols, full line). Left panel: central events. Right: peripheral collisions. Lines are drawn to guide the eye.

the opening of the multifragmentation channel has to be considered as a lower limit. This number is raised to about 9% if we consider the geometrical acceptance of the employed apparatus (about 83%), and a detailed estimation of the detection efficiency including energy thresholds would further increase it. The average calorimetric excitation energy for many-fragment events at $\cos(\theta_{flow}) \leqslant 0.5$ is 3 A MeV, very close to the total center of mass available energy.

3. Results

Fig. 4 displays the fragment ($Z \geqslant 3$) charge distribution measured for the two reactions in central (left) and peripheral (right) events. The superposition of the two peripheral data sets shows that our selection of peripheral events is effective in mainly isolating the QP, with minor contribution of QT decay.

A different behavior is observed in central collisions, where the charge distribution does not scale with the size of the system and an isospin effect can be envisaged, similarly to other experimental results [28].

Specifically, the source with the higher N/Z ratio (open symbols) leads to a more prominent U-shaped charge distribution. This can be intuitively justified considering that a high N/Z ratio of the source favors the production of large fragments, since such products are on average neutron rich. Therefore partitions consisting of a large heavy residue dominate. When the N/Z ratio is low (full symbols), the probability for a large cluster to survive is small and the system decays into lighter fragments, typically less neutron rich. The isospin dependence of the charge distributions also slightly influences the amount of three-fragment events in the two reactions. For the n-poor $^{32}\mathrm{S} + {}^{58}\mathrm{Ni}$ reaction the percentage of many-fragment events is 5%, while for the n-rich $^{32}\mathrm{S} + {}^{64}\mathrm{Ni}$ reaction is 3.5%.

As far as staggering is concerned, for both reactions a well pronounced odd–even effect is seen in the QP charge distribution, while almost no staggering appears neither in the fragment yield nor in the residue region for central collisions, where only an extra-production of carbon fragments is evident. This behavior has already been observed in many other reactions at low and intermediate incident energies, for central collisions [4,29–31].

In almost all the experiments quoted in Refs. [1,3] the experimental samples correspond mostly to peripheral collisions or to fission-fragment charge distributions. To our knowledge, no staggering has been directly observed in charge distributions for carefully selected central collisions [4]. Usually [1,4], the presence of odd–even effects are recovered by looking at the ratio of the charge distribution of a neutron-poor reaction and a neutron-rich one. In this way, however, the absolute value of the even–odd staggering for each reaction is lost.

As far as odd–even effects are concerned, the difference observed between central and peripheral collisions could tentatively be ascribed to a different isotopic ratio of the evaporating source as previously proposed in the literature [1,3,4].

However, another important difference between the two samples is given by the excitation energy, 3 A MeV on average in the central sample and less than half of this value for the peripheral sample. Such an important difference in the deposited energy could lead to different mechanisms for fragment production.

In addition, in the central sample (see Fig. 4) the huge variation of the production yields could "visually" mask odd–even effect. Indeed, the whole charge distribution for peripheral events changes only within one order of magnitude, while for central collisions it spans more than two orders of magnitude.

To verify these conjectures, we build the fragment charge distribution for events of the central sample, characterized by only two detected fragments and by $\cos(\theta_{flow})$ larger than 0.87. This selection produces in this event subset an average fragment relative velocity closely following the Viola systematics [32], showing that the selection is effective in isolating binary fission-like decays. In agreement with other experimental results [2,5] the even–odd staggering, shown in Fig. 5, becomes evident in this subset of central collisions, slightly more pronounced in the neutron-poor reaction.

This result means that an effect of the isospin content of the source exists, but that the fragment emission mechanism appears to be the dominant effect as far as staggering is concerned.

To corroborate this conclusion, we show in Fig. 6 the ratio between the elemental charge distribution of the whole central sample and a smoothed distribution obtained by a parabolic least squares interpolation of the measured yields over 5 consecutive points. From Fig. 6 it is evident that the staggering is present also in central collisions with amplitudes similar to the

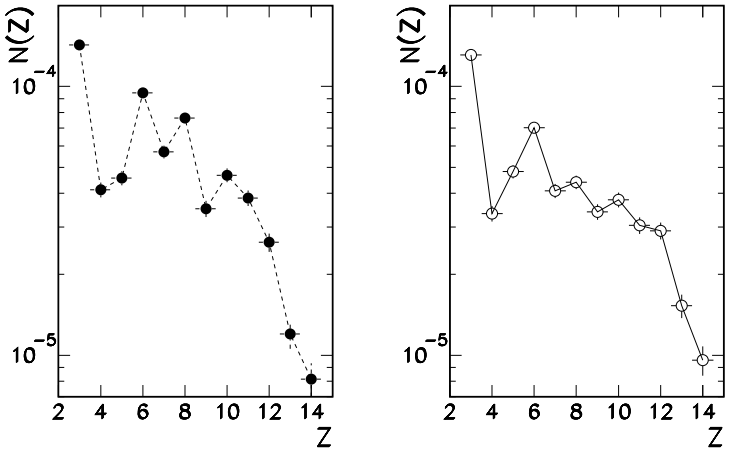

Fig. 5. Elemental fragment ($Z \geqslant 3$) distribution of the lightest fragment for central events with fragment multiplicity equal to 2. $^{32}S + ^{58}Ni$ (left) and $^{32}S + ^{64}Ni$ (right). Lines are drawn to guide the eye.

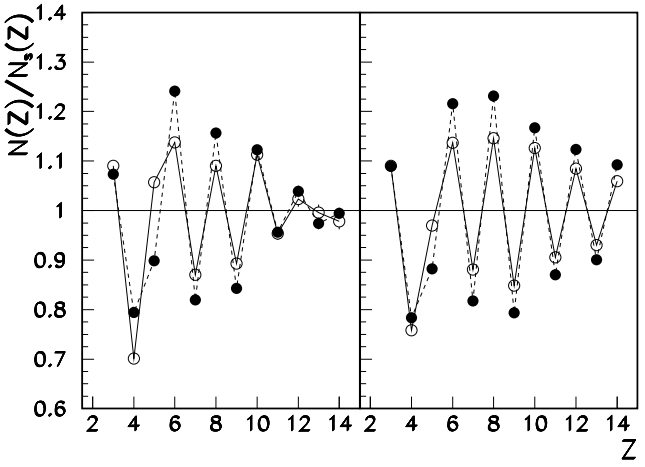

Fig. 6. Ratio of the elemental fragment ($Z \geqslant 3$) distribution of Fig. 4 for $^{32}S + ^{58}Ni$ (full symbols connected by dashed lines) and $^{32}S + ^{64}Ni$ (open symbols connected by full lines) by smoothed distributions obtained by a parabolic interpolation over 5 consecutive points. Left: central events. Right: peripheral collisions. Lines are drawn to guide the eye.

peripheral ones. Some extra differences between the two samples appear in this representation: the extra-production of carbon with respect to oscillations of neighboring charges is larger in central collisions and the amplitude of the staggering decreases for increasing fragment charge, at difference with peripheral events, where it remains almost constant.

For the two centrality selections the different isospin of the entrance channel plays a minor role, enforcing the idea that a different decay mechanism is at the origin of the observed differences between central and peripheral collisions. Specifically, only if the production yield as a function of the fragment size is reasonably smooth, a clear staggering can be visualized. This is the case of the binary central decays of Fig. 5 and, to a minor degree, of the peripheral samples.

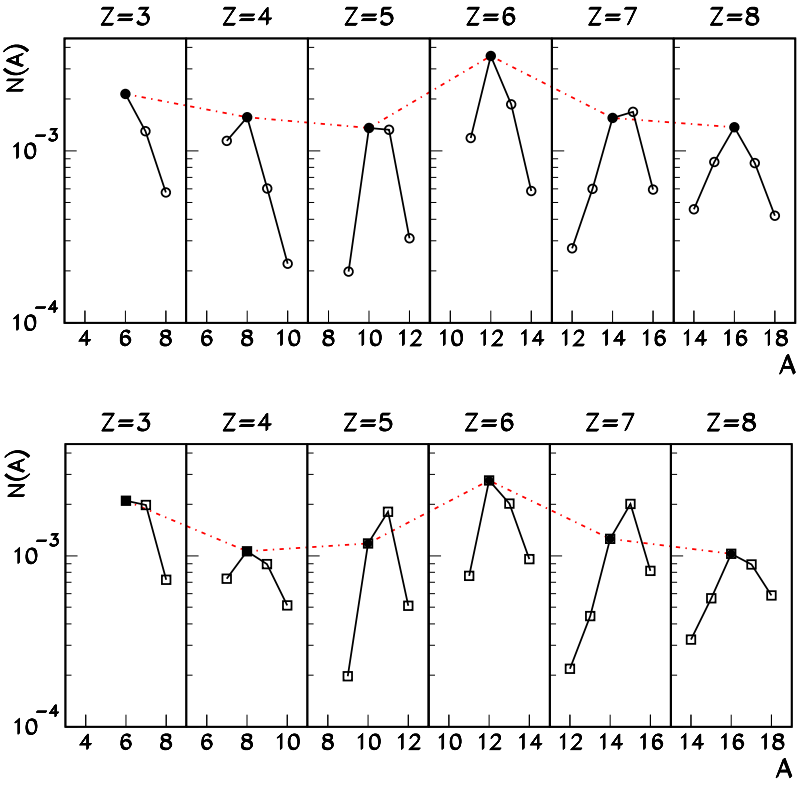

Fig. 7. (Color online.) Elemental isotopic distribution of $3 \leqslant Z \leqslant 8$ fragments for $^{32}S + ^{58}Ni$ (upper part) and $^{32}S + ^{64}Ni$ (lower part) for the peripheral sample. The solid symbols connected by a dot-dashed line correspond to the $N = Z$ isotopes.

In the case of whole set of the central events (Fig. 4) the strong variation of fragment yield, much larger than the staggering amplitude, does not allow to "visually" observe odd–even effects.

To investigate in more detail the influence of the excitation energy of the source in central collisions, a possible way would be to analyze data in excitation energy bins, but the statistics of the present data set is not sufficient. However we will have insights on this issue from model calculations in Section 4 below.

Let us now turn to examine staggering effects in the isotopic distributions. Since the staggering amplitude and features appear similar in peripheral and central collisions, once these latter are properly normalized, we limit this study to the peripheral sample. For this specific sample indeed not only odd–even effects appear more clearly, but also the statistics is sufficient to perform a complete analysis of isotopically resolved yields.

The isotopic distributions of the peripheral n-poor and n-rich system are displayed in Fig. 7. The ^{8}Be yield has been reconstructed through α–α correlation functions.[1]

[1] The reconstruction of the ^{8}Be yield is only partial, since in the present experiment the identification of isotopes is done via the energy loss in the silicon detector. Therefore a double-hit of two α-particles in the same strip of the silicon detector can be identified as Li, thus not contributing to the ^{8}Be yield.

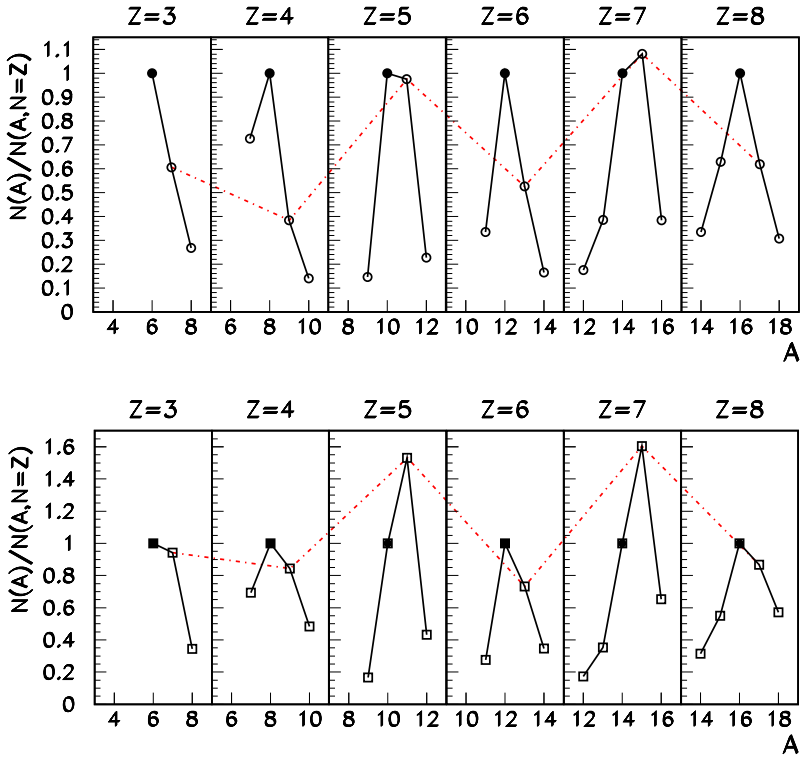

Fig. 8. (Color online.) Like Fig. 7 above, but normalized to the yield corresponding to $N = Z$ for each element. Symbols connected by a dot-dashed line correspond to the $N = Z + 1$ isotopes.

We can see that the neutron-rich system tends to produce neutron-rich fragments suggesting that some isospin diffusion has taken place in the collision. In most cases the most abundant isotope is $N = Z$, meaning that the staggering observed in the global distributions Fig. 6 can indeed be interpreted as a dominance of even–even isotopes over odd–odd ones as one might naively expect from a pairing effect.

To see the isotopic effect on the staggering, it is useful to normalize the isotopic yields to the one corresponding to $N = Z$ for each element, as shown in Fig. 8. Some systematic trends appear with this representation. Specifically n-poor isotopes ($N = Z - 1$) are more abundant for even Z than for odd Z, while n-rich isotopes ($N = Z + 1$ and $N = Z + 2$) are more abundant for odd Z than for even Z.

These isotopic effects appear more clearly if the elemental yields are sorted as a function of $N - Z$ values (isotopic chains) as proposed by the GSI group [3]. As for the discussion of the elemental distributions above, the non-monotonic behavior of the mass distribution shown in Fig. 7 is superimposed to the isotopic effect, partially masking the odd–even fluctuations. To disentangle the two effects and provide a better evidence of the isotopic behavior, it is useful to normalize the measured yield of each isotope to the total detected yield for the considered element.

This normalized distribution, defined as:

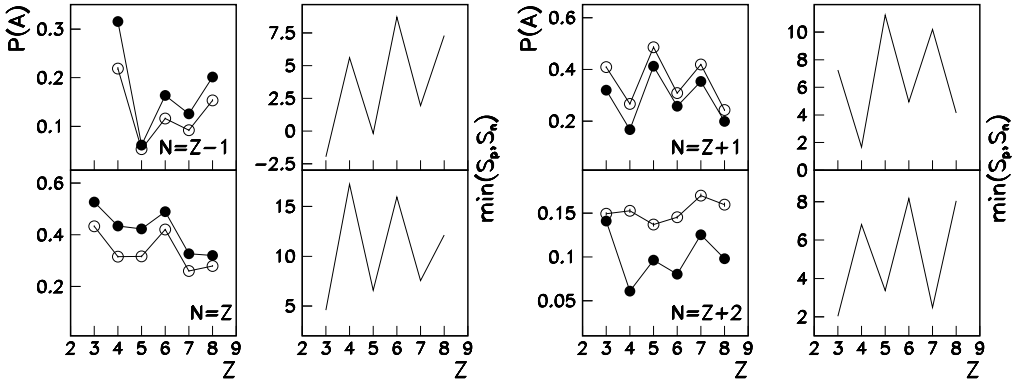

Fig. 9. Normalized distribution of $3 \leqslant Z \leqslant 8$ fragments for $^{32}S + {}^{58}Ni$ (full symbols) and $^{32}S + {}^{64}Ni$ (open symbols) for peripheral collisions corresponding to different isotopic chains. For each chain, the panels on the right show the corresponding behavior of the fragment lowest nucleon emission threshold (see text).

$$P(A, Z) = \frac{Yield(A, Z)}{\sum_A Yield(A, Z)} \tag{3}$$

is presented in the left panels of Fig. 9 for the two reactions.

The behavior of the $N = Z$ yields is confirmed by this procedure, while odd–even effects appear more clearly for the other isotopic chains, that correspond to lower cross sections.

As proposed by Ricciardi et al. [3], the observed trend is qualitatively compared to the behavior of the lowest particle emission threshold, i.e. the lowest between the proton and neutron separation energies of the final daughter nucleus.

In agreement with FRS data, the behavior of the isotopic distributions is qualitatively similar to the behavior of the lowest separation energy, suggesting that the last (neutron or proton) evaporation step might be at the origin of the observed staggering, as it is proposed by the authors of Ref. [3]. An exception is however given by the $N = Z + 2$ isotopic chain, which shows a reversed staggering with respect to the separation energies.

This interpretation moreover requires that the last evaporation step is completely dominated by the competition between proton and neutron emission. This is clearly not the case for the ^{8}Be yield, which has been reconstructed through α–α correlations, and the same may be true for other isotopes.

To have a more global view of the issue, Fig. 10 displays the Q-values for neutron, proton and α-decay for the different isotopic chains [33]. The lowest Q-value for the $N = Z$ chain typically corresponds to α-decay (with the only exception of ^{14}N) and this quantity does not show any oscillating trend as a function of Z. This rather flat pattern for the α-particle separation energy is present for all the other isotopic chains.

The position of the first particle-unstable excited level of the nucleus is also shown in Fig. 10 [33], and nicely coincides with the lowest Q-value. Looking at the position of the first particle-unstable excited level for nuclei of all the isotopic chains we can formulate other interesting considerations, which make us believe that the information on the characteristics of the daughter nuclei should be complemented by taking into account the characteristics of the parent nuclei they were originated from, in particular their level density and their separation energy.

In the case of $N = Z + 1$ parent nuclei we see that even-Z nuclei in their first particle-unstable excited level decay by n emission, and the corresponding daughter are even-Z $N = Z$ isotopes, while odd-Z nuclei decay mainly by α emission (with the exception of ^{15}N), corresponding to

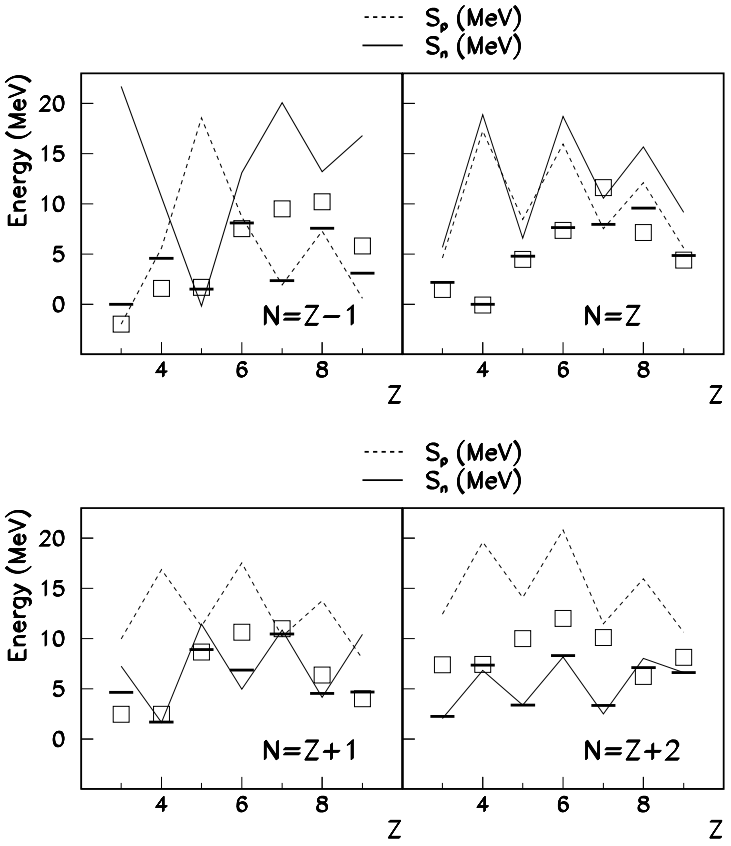

Fig. 10. Comparison of the energy of the lowest unstable state (thick lines) decaying in a given daughter isotope, with the Q-value for α-decay (open squares) and the neutron (S_n) and proton (S_p) separation energies.

daughters with odd-Z and of the same $N = Z+1$ class. Moreover, since the first particle-unstable excited level for even-Z nuclei lies at a lower energy with respect to the first level of odd-Z ones, we could say that even-Z nuclei are produced in their excited levels with a higher probability. Since the decay from this level is determined in a quasi-deterministic way by energy thresholds, the higher probability for the excitation of the first level in ^{9}Be, ^{13}C and ^{17}O as parent nuclei will translate into an increased yields for ^{8}Be, ^{12}C and ^{16}O daughter, which is seen in the data.

In the case of $N = Z+2$ parent nuclei the energy position of the first particle-unstable excited level follows exactly the trend of $\min(S_n, S_p)$, and, with the exception of ^{18}O, all the levels are unstable against n-emission. This means that, considering parent nuclei of the type $N = Z+2$, their daughters would be all $N = Z+1$ nuclei. Moreover, since the levels of even-Z nuclei lie at a higher energy with respect to the odd-Z ones, we expect an increase in the yield of odd-Z $N = Z+1$ nuclei, which is seen in the data.

As far as $N = Z+2$ daughter nuclei in the final yields are concerned, the interpretation of Fig. 10 is not so straightforward. Nuclei of this kind could come for instance from the proton decay of $N = Z+1$ nuclei with excitation energies higher than the one corresponding to the first particle-unstable excited state. In this case the proton separation energies for $N = Z+1$ show an oscillation coherent with the oscillation of the measured $N = Z+2$ yields, under the hypothesis

of a lower probability for an excitation at a higher energy. But $N = Z + 2$ nuclei could also come from the α-decay of nuclei of the same $N = Z + 2$ class: in this case no oscillating trend is observed for the Q-value for α-decay, but the α-decay threshold for $Z = 6$ is higher than that for the neighboring nuclei, suggesting an underproduction of $Z = 6$ nuclei of the class $N = Z + 2$. The same holds if we consider $N = Z + 2$ nuclei as daughter of the neutron decay of $N = Z + 3$ parents.

Finally, the case $N = Z - 1$ of Fig. 10 shows that the lowest Q-value for the first particle-unstable excited level of parent nuclei corresponds to α-decay, with the exceptions of ^{13}N, ^{15}O and ^{17}F, which decay by emission of a proton and a daughter fragment with $N = Z$, increasing the yield of $N = Z$ nuclei, observed in the data.

Concluding, the presence of staggering in the final measured yields can be linked to the population of the parent nuclei at the previous steps of the decay chain and cannot be fully explained by the behavior of the lowest particle emission threshold of the final daughter nuclei.

4. Insights from statistical models

Further insights on odd–even effects can be gained from statistical model calculations.

Because of the limited excitation energy, our peripheral sample can be reasonably described as a standard Hauser–Feshbach or Weisskopf evaporation from an excited source of mass and charge close to the projectile. This emitting source is not well defined in the experimental data because different impact parameters are summed up, neutrons are not measured and the statistics is too poor to make precise selections in the source characteristics. This means that data have to be seen as a superposition of different mass, isospin, angular momentum and excitation.

Because of this experimental limitation we have not tried a quantitative comparison between model and data. The purpose of the calculation being simply to enlighten the physical mechanism leading to the presence (absence) of odd–even effects in the different thermodynamic conditions, we have simply fixed in the GEMINI [34] evaporation model a source with Gaussian-distributed parameters with $\langle E^* \rangle = 1$ A MeV, $\sigma_E* = 0.1$ A MeV, $\langle Z \rangle = 16$ and $\sigma_Z = 1$. The source mass number is then fixed as $A = 2Z$. Concerning the angular momentum, we have considered a triangular distribution between $J_{\min} = 0\hbar$ and $J_{\max} = 16\hbar$, the maximum value of L compatible with this low excitation energy.

The results for the different isotopic chains as well as the inclusive distributions are reported in Fig. 11. We can see that the overall shape of the theoretical distribution is in relatively good agreement with the experimental data (see Fig. 4 above), confirming the essential statistical character of QP decay.

Clear staggering effects are seen in the QP-remnants region, especially in the $N = Z$ isotopic chain, where unfortunately we do not have isotopic discrimination in the experiment. Since in the model calculation $N = Z + 1$ nuclei are the most abundant isotopes in the residue region and their distribution is essentially smooth, the inclusive theoretical distribution does not show any noticeable odd–even effect in this region, while odd–even effects appear slightly more clearly in the experiment.

Concerning the fragment region ($3 \leqslant Z \leqslant 8$), where the isotopic information is accessible experimentally, a good qualitative agreement is observed for $N = Z - 1$ and $N = Z$ but deviations can be seen for $N = Z + 1$, which again is essentially flat in the calculation.

To disentangle the information of the production cross section from the information on staggering effects, the right part of Fig. 12 displays the ratio between the elemental charge distribution obtained by the GEMINI model and a smoothed distribution obtained by a parabolic interpola-

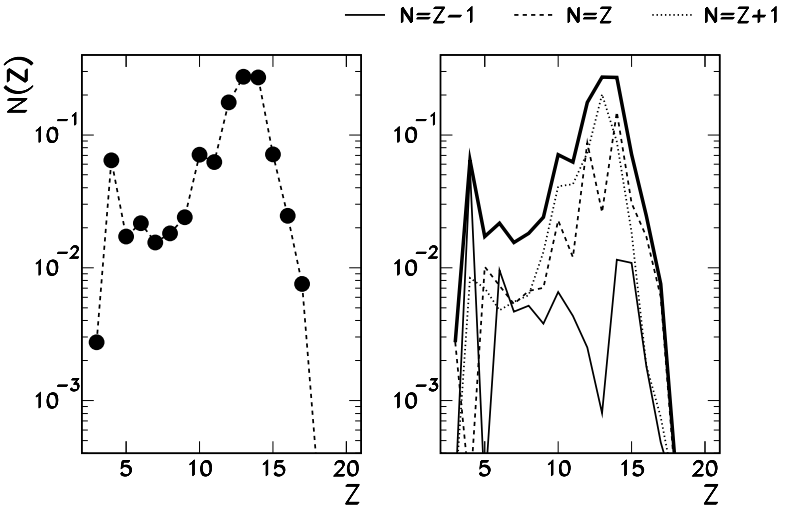

Fig. 11. Elemental asymptotic distribution from the decay of an excited source with $\langle A\rangle = 32$, $\langle Z\rangle = 16$, $\langle E^*\rangle = 1$ A MeV and a triangular distribution of angular momentum between $J = 0\hbar$ and $J = 16\hbar$, within the GEMINI evaporation model. Left panel: inclusive charge distribution. Right panel: distribution for different isotopic chains.

tion of the calculated yields over 5 consecutive points, to be compared with the experimental data Fig. 6 above. We can see that the qualitative agreement is good.

The most important discrepancy concerns the relative yield of Li and Be isotopes, which is inverted in the calculation respect to the trend shown by the experiment. Different explanations can be invoked to understand this discrepancy. First, the GEMINI code makes a switch from the Hauser–Feshbach formalism, used to describe light nuclei ($Z \leqslant 3$) evaporation, to the Bohr–Wheeler formalism, used to treat the emission of complex fragments heavier than Li. The absence of a unified description of fission and evaporation may be at the origin of the observed discrepancy. Moreover, the Be/Li ratio in the Gemini code is sensitive to the value of the maximal angular momentum, which is poorly constrained in the experimental sample. Finally, a pre-equilibrium contribution of the measured Li yield in peripheral events cannot be excluded.

In conclusion, our peripheral events appear to be consistent with the evaporative decay of QP sources. The staggering of the elemental distribution is qualitatively reproduced by the calculation, even if differences appear when the behavior is analyzed in different isotopic chains.

A more quantitative comparison would need a better determination of the experimental source characteristics, needed as input of the GEMINI model, which is out of scope of the present analysis.

All the observables presented in this section keep the original information, provided that model events, filtered through the software replica of the experimental apparatus, are selected by the condition that at least 70% of the initial charge is detected.

Now let us turn to the analysis of the central collisions. Since the experimental sample does not correspond to complete fusion of projectile and target, fluctuations arise from the mixing of events with different degrees of mass and energy transfer. For this reason, similarly to the case of binary collisions, we have not tried a quantitative comparison to experiment but considered the statistical decay of a Gaussian-distributed source, with $\langle Z\rangle = 40$, $\sigma_Z = 1$, $\langle E^*\rangle = 3$ A MeV, $\sigma_E = 0.1$ A MeV. The source mass numbers are assumed $A = 2Z + 1$ and $A = 2Z + 7$, in agreement with the predictions of the Hipse dynamical event generator [26] for the $^{32}\mathrm{S} + {}^{58}\mathrm{Ni}$

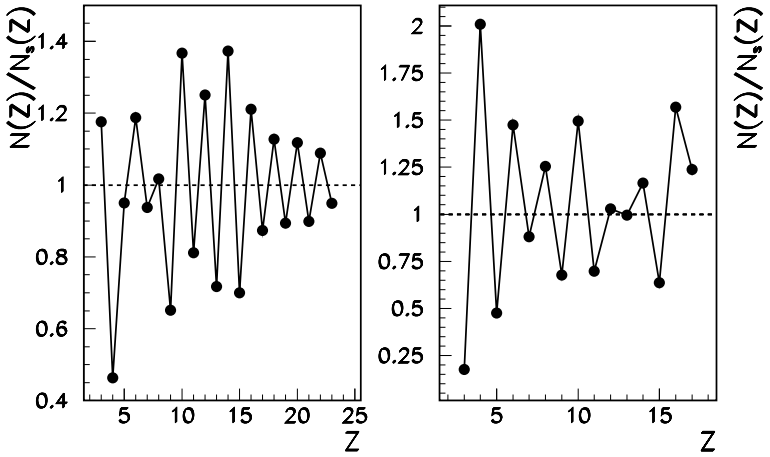

Fig. 12. Ratio of the elemental fragment ($Z \geqslant 3$) distribution of the GEMINI simulations by smoothed distributions obtained by a parabolic interpolation over 5 consecutive points. Left: central events (see the calculation with $J_{\max} = 56\hbar$ in Fig. 13). Right: peripheral collisions (see Fig. 11). Lines are drawn to guide the eye.

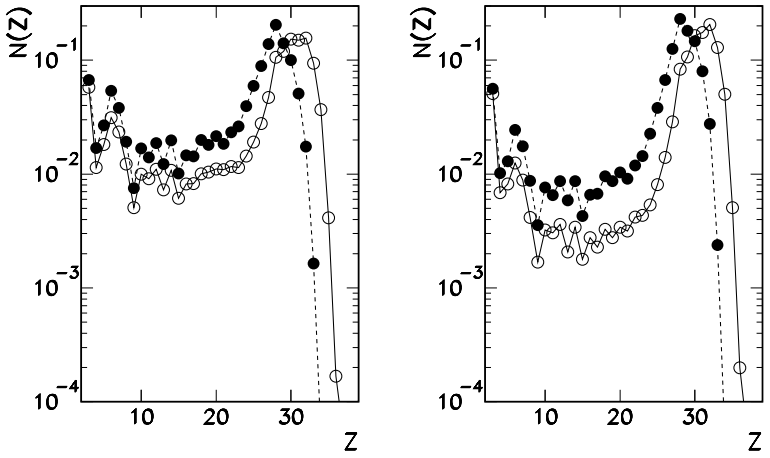

Fig. 13. Elemental asymptotic distribution from the decay of an excited source with $\langle A \rangle = 81$, $\langle Z \rangle = 40$, $\langle E^* \rangle = 3$ A MeV (full symbols, dashed lines) and $\langle A \rangle = 87$, $\langle Z \rangle = 40$, $\langle E^* \rangle = 3$ A MeV (open symbols, full lines) within the GEMINI evaporation model. For both sources the angular momentum ranges from $J = 0\hbar$ to $J = J_{\max}$ with a triangular distribution. Left: $J_{\max} = 56\hbar$; right: $J_{\max} = 40\hbar$.

and $^{32}\mathrm{S} + {}^{64}\mathrm{Ni}$ reactions, where the incomplete fusion of the projectile and targets happens at impact parameters smaller than 3 fm.

Since the angular momentum is not constrained by the data, we run the GEMINI code with a triangular distribution of J, with maximum value $J_{\max} = 56\hbar$, corresponding to the maximum impact parameter for the incomplete fusion.

Fig. 13 displays the inclusive charge distributions obtained from the GEMINI model for the two assumed sources, to be compared with the data shown in Fig. 4.

As in the case of the experimental sample the source with the higher N/Z ratio (open symbols) leads to a heavier residue with respect to an n-poor source (full symbols). The production of

fragments lighter than the residue is modified in the model by the isospin of the source similarly to the data. In particular the two distributions differ of a factor 2 in the range of charges $8 \leqslant Z \leqslant 15$, both in the model and in the data.

Clear staggering effects can be seen in the calculation for the region of complex fragments ($Z < 15$), very similar to the case of the QP source. The variation of the angular momentum does not change the overall shape of the distribution, nor the importance of the odd–even effects. This confirms the expectation [3] that, in an evaporation based picture, odd–even effects do not depend on the initial excitation energy and are essentially determined by the last evaporation step(s). At a more quantitative level, these effects appear much more important than in the experimental sample. As we have discussed in Section 2, this might be due to the different shape of the distribution, since the theoretical predictions are flatter in the range $10 \leqslant Z \leqslant 20$ than the measured ones. To demonstrate this statement, the GEMINI yield is again normalized to the smoothed one in the left part of Fig. 12. Comparing to Fig. 6 above, we can notice that odd–even effects are too strong in the calculation, and disappear at much higher charges than experimentally observed. However it is clear that the global structure of the odd–even effect is very well reproduced by the calculation, particularly the decreasing trend with increasing charge.

These differences indicate that the main source of disagreement between the model and the data lies in the incorrect prediction of the production yields, and this has a non-negligible influence on the absolute value of the staggering. This may not be surprising considering that at the excitation energy corresponding to the central sample a simple evaporation scenario may not be adequate.

In particular, the experimental fragment production for the range $10 \leqslant Z \leqslant 20$, is about a factor 4 less than in the model distributions of Fig. 13 if $J_{\max} = 56\hbar$ is assumed. We can approximately recover the experimental fragment production by limiting the maximum angular momentum in GEMINI at $40\hbar$, as it is shown in the right part of Fig. 13. However it may be interesting to notice that the fraction of three-fragment events is about 0.5% if the angular momentum is decreased, an order of magnitude too small with respect to the uncorrected data. This is an indication that a fragment emission mechanism different from the GEMINI sequential binary decay might be present in the experimental sample, and have an influence on the fragment production yields and consequently on the odd–even effects.

A further indication in this sense is given by Fig. 14, which shows the relative velocity distribution between the two heaviest fragments, in events where at least three fragments with $Z \geqslant 3$ are present. This velocity is peaked at the predicted value from the Viola systematics [32] in the GEMINI model, as expected from a sequence of binary decays. Conversely, the experimental data show higher relative velocities, pointing to a different emission mechanism [35].

These discrepancies may be understood from the opening of the simultaneous multifragmentation channel, which is not accounted for in the GEMINI model and would be better described by a multifragmentation model.

Unfortunately, some of the existing multifragmentation models [36,37] very successful in reproducing in detail static as well as dynamical characteristics of fragment production for excited sources with excitation energies comparable to the present sample [38], treat nuclear clusters as liquid drops. They do not take into account neither shell and pairing effect in their mass, nor the discrete particle unstable spectrum in all stages of the compound nucleus decay, the justification being that these models are supposed to be realistic only above the multifragmentation threshold, where structure effects are washed out. As a consequence, model distributions are smooth by construction and no insight about the presence/absence of odd–even effects can be gained from these calculations. An interesting attempt to include structure effects in multifragmentation

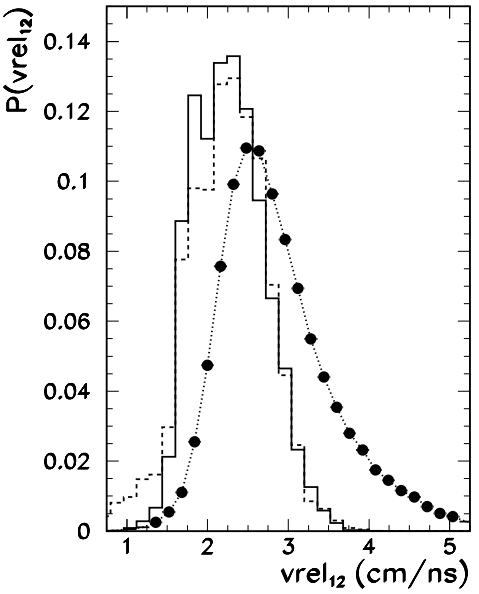

Fig. 14. Experimental distribution of the relative velocity of the two largest fragments, for central events with at least three fragments ($Z \geqslant 3$) (solid symbols, dotted line). Solid line is the GEMINI distribution for the decay of an excited source $\langle A \rangle = 81$, $\langle Z \rangle = 40$, $\langle E^* \rangle = 3$ A MeV. Dashed line is the GEMINI filtered distribution. All distributions have been normalized to unit area.

models was proposed in Ref. [39], and it would be very interesting to see if this model can better describe our data.

It is important to stress that the multifragmentation process in itself cannot be at the origin of the observed discrepancy, given the low probability observed for three-fragment events in this data set. However the so-called "multifragmentation" models can give different predictions also of binary events, with respect to fission–evaporation models like GEMINI. This is mainly due to the fact that in multifragmentation models [40] the probability of a binary split is evaluated from the density of states at the scission point, and not at the saddle point as in the standard Bohr–Wheeler formalism which is implemented in the GEMINI model [41].

In any case the failure of the standard fission–evaporation picture at these high excitation energies suggests that the emission mechanism plays an important role for the light fragment yield, and/or that their decay is not governed by Q-values only.

5. Conclusions

In this paper we have reported on an experimental study of staggering in $^{32}S + ^{58}Ni$ and $^{32}S + ^{64}Ni$ collisions at 14.5 A MeV, performed with the TANDEM-ALPI acceleration system at the Legnaro National Laboratory. The data collection was assured by the GARFIELD apparatus coupled to a high resolution annular detector for correlation measurements, the Ring Counter. Thanks to the important angular coverage and the low detection thresholds, we have been able to select two main classes of dissipative events for each reaction, corresponding to the statistical decay of an excited quasi-projectile, and of an incomplete fusion source respectively. Important odd–even effects are seen over the whole range of fragment charge, included the QP remnants

yields, for peripheral collisions, while these effects seem at a first glance much less important in the central collision sample.

This different behavior can be understood as an effect of the different de-excitation mechanism in peripheral and central collisions. The opening of the multifragmentation channel in this relatively light system leads to a characteristic yield distribution which, varying rapidly with the fragment size, hides the relatively smaller amplitude of odd–even effects. The multifragmentation yields cannot be reproduced by statistical models where ternary events are obtained as successive binary decays. Only if the yields are properly renormalized such as to compensate for this effect of the emission mechanism, odd–even effects can be recovered and some systematic trends appear. Specifically, the staggering is more pronounced in neutron-poor systems and reduces with increasing fragment charge if the excitation energy is high.

This feature, together with a detailed study of the most probable decay channel for the different isotopic chains, suggests that odd–even staggerings depend on the whole evaporation chain and not only on the energy balance of the last evaporation step. This conclusion is in agreement with other experimental results in the low or intermediate energy domain [4–6].

To confirm (or infirm) this statement, a detailed comparison with statistical models will be needed. To this aim, a necessary improvement concerns the coupling between multifragmentation and the subsequent evaporation of excited primary fragments, where a consistent and realistic treatment of the fragment energy functional should be employed, including pairing effects, realistic level densities and the discrete particle unstable spectrum in both regimes of the compound nucleus decay.

Acknowledgements

The authors are indebted to R. Cavaletti, A. Paolucci and L. Costa for the technical support during the experiment, M. Loriggiola for preparing the targets and M. Ottanelli for having realized the target-holder control system.

The authors also wish to thank the accelerator staff of the TANDEM-ALPI complex of LNL (Laboratori Nazionali di Legnaro) for having provided high quality beams.

One of the authors (Ad.R.R.) gratefully acknowledges the kind hospitality of INFN-Sezione di Bologna, where the work was partially done.

This work was supported in part by grants of Alma Mater Studiorum (Bologna University).

References

[1] L.B. Yang, et al., Phys. Rev. C 60 (1999) 041602 and references quoted therein.
[2] Sl. Cavallaro, et al., Phys. Rev. C 57 (1998) 731.
[3] M.V. Ricciardi, et al., Nucl. Phys. A 733 (2004) 299;
M.V. Ricciardi, et al., arXiv:1007.0386v1.
[4] E. Geraci, et al., Nucl. Phys. A 732 (2004) 173.
[5] E. Bonnet, J.P. Wieleczko, et al., Int. J. Mod. Phys. E 17 (2009) 2359.
[6] G. Cardella, Limiting Collaboration, private communication;
I. Lombardo, et al., Int. J. Mod. Phys. E 20 (2011) 1066.
[7] R. Kumar, R.K. Gupta, Phys. Rev. C 79 (2009) 034602;
R.K. Gupta, et al., J. Phys. G 32 (2006) 345.
[8] A. Schiller, et al., Phys. Rev. C 63 (2001) 021306(R).
[9] N. Chamel, et al., Phys. Rev. C 81 (2010) 045804.
[10] A. Fantina, et al., Phys. Lett. B 676 (2009) 140.
[11] M. Colonna, F. Matera, Phys. Rev. C 71 (2005) 064605.

[12] A. Ono, AIP Conf. Proc. 884 (2007) 292.
[13] J. Su, et al., Phys. Rev. C 83 (2011) 014608.
[14] S. Wuenschel, et al., Phys. Rev. C 79 (2009) 061602(R).
[15] Ad.R. Raduta, F. Gulminelli, Phys. Rev. C 75 (2007) 044605.
[16] R. Charity, et al., Phys. Rev. C 63 (2001) 024611.
[17] A. Kelic, M.V. Ricciardi, K.H. Schmidt, arXiv:0906.4193.
[18] V. Ricciardi, private communication.
[19] J.B. Natowitz, et al., Phys. Rev. C 65 (2002) 034618.
[20] F. Gramegna, et al., Nucl. Instr. Meth. A 389 (1997) 474;
F. Gramegna, et al., in: IEEE Nucl. Science Symposium, Rome, 16–22 October, 2004.
[21] A. Moroni, et al., Nucl. Instr. Meth. A 556 (2006) 516.
[22] J. Cugnon, D. L'Ĥote, Nucl. Phys. A 397 (1983) 519.
[23] N. Marie, et al., Phys. Lett. B 391 (1997) 15.
[24] M. D'Agostino, et al., Phys. Lett. B 368 (1996) 259.
[25] V. Metivier, et al., Nucl. Phys. A 672 (2000) 357.
[26] D. Lacroix, et al., Phys. Rev. C 69 (2004) 054604.
[27] G. Casini, et al., Phys. Rev. Lett. 71 (1993) 2567;
J. Toke, et al., Phys. Rev. Lett. 75 (1995) 2920;
S. Piantelli, et al., Phys. Rev. Lett. 88 (2002) 052701.
[28] F. Amorini, et al., Phys. Rev. Lett. 102 (2009) 112701.
[29] F. Gramegna, et al., Fizika B 12 (1) (2003) 39.
[30] M.B. Tsang, Eur. Phys. J. A 30 (2006) 129;
M.B. Tsang, Eur. Phys. J. A 32 (2007) 243, Erratum.
[31] F. Saint-Laurent, INDRA Collaboration, Nucl. Phys. A 583 (1995) 481.
[32] V. Viola, Phys. Rev. C 31 (1985) 1550.
[33] http://www.nndc.bnl.gov/nudat2/.
[34] R.J. Charity, Phys. Rev. C 82 (2010) 014610.
[35] B. Davin, et al., Phys. Rev. C 65 (2002) 064614.
[36] J.P. Bondorf, A.S. Botvina, A.S. Iljinov, I.N. Mishustin, K. Sneppen, Phys. Rep. 257 (1995) 133.
[37] Al.H. Raduta, Ad.R. Raduta, Phys. Rev. C 55 (1997) 1344;
Al.H. Raduta, Ad.R. Raduta, Phys. Rev. C 65 (2002) 054610.
[38] M. D'Agostino, et al., Nucl. Phys. A 650 (1999) 329;
M. D'Agostino, et al., Nucl. Phys. A 724 (2003) 455.
[39] W.P. Tan, et al., Phys. Rev. C 68 (2003) 034609.
[40] A.J. Cole, Statistical Models for Nuclear Decay, IOPP, Bristol, 2000.
[41] D. Mancusi, et al., Phys. Rev. C 82 (2010) 044610.